some of us (Gallois *et al.*, 1983). This is true whether the disorder is due to the method of preparing the samples or to the application of a constraint. This observation suggests that the condition of the appearance of a distortion in the lattice is the existence of a triperiodic iodine lattice. Nevertheless it has not been possible to establish more precisely the relations between the superstructure and the degree of iodine order.

The authors are very indebted to P. Dupuis (Laboratoire de Chimie Physique Macromoléculaire, Nancy, France) who kindly provided the samples and thank C. Coulon (Centre de Recherche Paul Pascal, Talence, France) for very helpful discussions.

### References

ABKOWITZ, M. A., EPSTEIN, A. J., GRIFFITHS, C. H., MILLER, J. S. & SLADE, M. L. (1977). *J. Am. Chem. Soc.* **99**, 5304-5308.
ANDRÉ, A., FOURME, R. & RENAUD, M. (1971). *Acta Cryst.* B**27**, 2371-2380.
BRILL, J. W., EPSTEIN, A. J. & MILLER, J. S. (1979). *Phys. Rev. B*, **20**, 681-685.
COPPENS, P., LEUNG, P., MURPHY, K. E., TILBORG, P. R., EPSTEIN, A. J. & MILLER, J. S. (1980). *Mol. Cryst. Liq. Cryst.* **61**, 1-6.
COUGRAND, A., FLANDROIS, S., DELHAES, P., CHASSEAU, D., GAULTIER, J. & MIANE, J. L. (1976). *Mol. Cryst. Liq. Cryst.* **32**, 165-170.
COULON, C. (1983). Ph.D. Thesis. Univ. of Bordeaux I, France.
COULON, C., FLANDROIS, S., DELHAES, P., HAUW, C. & DUPUIS, P. (1981). *Phys. Rev. B*, **23**, 2850-2859.
DUPOUY, G. (1974). *Proceedings of the 3rd International Conference on High Voltage Electron Microscopy*, edited by P. R. SWANN, C. J. HUMPHREYS & M. J. GORINGE, pp. 441-457. London: Academic Press.
DUPUIS, P., FLANDROIS, S., DELHAES, P. & COULON, C. (1978). *J. Chem. Soc. Chem. Commun.* pp. 337-338.
FILHOL, A., GALLOIS, B., LAUGIER, J., DUPUIS, P. & COULON, C. (1982). *Mol. Cryst. Liq. Cryst.* **84**, 17-29.
FILHOL, A. & GAULTIER, J. (1980). *Acta Cryst.* B**36**, 592-596.
FILHOL, A., ROVIRA, M., HAUW, C., GAULTIER, J., CHASSEAU, D. & DUPUIS, P. (1979). *Acta Cryst.* B**35**, 1652-1660.
FLANDROIS, S., COULON, C., DELHAES, P., CHASSEAU, D., HAUW, C., GAULTIER, J., FABRE, J. M. & GIRAL, L. (1981). *Mol. Cryst. Liq. Cryst.* **14**, 663.
GALLOIS, B., COULON, C., POUGET, J. P., FILHOL, A. & DUPUIS, P. (1984). In preparation.
GALLOIS, B., GAULTIER, J., POUGET, J. P., COULON, C. & FILHOL, A. (1983). *J. Phys. C*, **3**, 1307-1312.
GRANIER, T. (1982). Thesis. Toulouse, France.
GRANIER, T. & AYROLES, R. (1982). *J. Phys. (Paris) Lett.* **43**, L285-L290.
GRANIER, T. & AYROLES, R. (1983). *J. Phys. C*, **3**, 1301-1306.
GUINIER, A. (1964). *Théorie et Techniques de la Radiocristallographie*, p. 523. Paris: Dunod.
IKARI, T., JANDL, S. & AUBIN, M. (1983). *Phys. Rev. B*, **28**, 3859-3863.
KHANNA, S. K., POUGET, J. P., COMÈS, R., GARITO, A. F. & HEEGER, A. J. (1977). *Phys. Rev. B*, **16**, 1468-1479.
MEGTERT, S., POUGET, J. P., COMÈS, R., GARITO, A. F., BECHGAARD, K., FABRE, J. M. & GIRAL, L. (1978). *J. Phys. (Paris) Lett.* **39**, L118-L121.
SALIH, S. M. & COSSLETT, V. E. (1975-1976). *Development in Electron Microscopy and Analysis*, edited by J. A. VENABLES, pp. 311-314. London: Academic Press.
SHCHEGOLEV, I. F. (1972). *Phys. Status Solidi A*, **12**, 9-45.
THOMAS, L. E., HUMPHREYS, C. J., DUFF, W. R. & GRUBB, D. T. (1970). *Radiat. Eff.* **3**, 89-91.
YAMAJI, K., MEGTERT, S. & COMÈS, R. (1981). *J. Phys. (Paris)*, **42**, 1327-1343.
YAMAJI, K., POUGET, J. P., COMÈS, R. & BECHGAARD, K. (1983). *J. Phys. (Paris) Colloq.* C**3**, 1321-1323.
ZUPPIROLI, L. & BOUFFARD, S. (1980). *J. Phys. (Paris)*, **41**, 291-297.
ZUPPIROLI, L., MUTKA, H. & BOUFFARD, S. (1982). *Mol. Cryst. Liq. Cryst.* **85**, 1391-1409.

*Acta Cryst.* (1985). B**41**, 66-76

# Chain Ordering in $E_2PI_{1.6}$ (5,10-Diethylphenazinium Iodide)

BY E. ROSSHIRT, F. FREY, H. BOYSEN AND H. JAGODZINSKI

*Institut für Kristallographie und Mineralogie der Universität München, Theresienstrasse* 41, *D* 8000 *München* 2, *Federal Republic of Germany*

(*Received* 4 *April* 1984; *accepted* 14 *August* 1984)

### Abstract

X-ray diffraction patterns of the title compound reveal long-range, short-range and disorder phenomena due to different interactions between and within two sublattices which are incommensurate with one another. A prominent system of diffuse layer lines is due to chain-like inclusions of polyiodide anions. At room temperature doubled and sixfold superperiods along the chains are superimposed. The organic matrix shows a fourfold superstructure along the stacking direction. Lateral correlations are of both short- and long-range type. The description in a frame of uncorrelated sublattices becomes worse at low temperatures ($\lesssim$190 K). The main diffuse system has been analysed in terms of one-dimensional liquid models. The best quantitative agreement was found for an asymmetric distribution function of next-nearest $I_3$ units, which is intermediate between the classical Zernike-Prins model and a symmetric Gaussian distribution. The

0108-7681/85/010066-11$01.50 

temperature dependence was studied between 183 and 333 K, where the mean distance and its mean square deviation decrease with decreasing temperature from 9·87 to 9·80 Å and from 0·36 to 0·17 Å, respectively.

## 1. Introduction

Highly anisotropic structural and physical properties are found in compounds with chain-like inclusions which are currently under investigation in connection with one-dimensional (1D) order problems, incommensurate phenomena, chemical bonding, superconductivity, excitations in 1D systems, *etc.* Among them there is a class of solids containing linear chains of polyiodide anions surrounded by stacks of oxidized organic molecules (see, for example, Hoffmann, Martinsen, Pace & Ibers, 1982). $E_2PI_{1\cdot6}$, first synthesized by Endres, Harms, Keller, Moroni, Nöthe, Vartanian & Soos (1979), belongs to this class. In a framework built by columnar stacks of $C_{16}H_{18}N_2^+$ ($E_2P$) molecules channels are left open in which the iodine-anion chains are embedded. As reported by Endres *et al.* (1979) and Endres (1980) the *c* periods along the unique axis of the organic matrix and of the iodine chains, respectively, are incommensurate with one another, at least at room temperature.

The results of the structure determination (Endres *et al.*, 1979; Endres, 1980) can be summarized as follows: The averaged structure of the organic matrix belongs to space group $P42_12$ ($a = 12{\cdot}321$, $c_o = 5{\cdot}330$ Å). Stacks of planar but tilted $E_2P$ cations run parallel to **c** (Fig. 1*a*). No convergence could be reached in the structure refinement which stopped at $R \sim 10{\cdot}1\%$. Concerning the iodine chains a projection along **c** forms a well ordered centred lattice according to the well defined channels. From the diffuse layer system a repeat period of $c_1 = 9{\cdot}70$ Å can be evaluated, although long-range order does not exist. Structural units of the chains are $I_3^-$ ions as found from resonance Raman experiments (Dietz & Sunder; cited in Endres, 1980) and also from the relatively high intensity of the 3rd, 6th,... diffuse layer. In a 1D structure determination the more or less diffuse layer lines were treated by Endres (1980) as 1D Bragg peaks. From integrated intensities a structural parameter $u = 0{\cdot}027$ was determined which defines a mean I–I distance of $(\frac{1}{3} - u)c_1 = 2{\cdot}97$ Å within an $I_3$ unit (Fig. 1*b*). In addition to difficulties with a clear definition of the integrated intensities the interpretation itself suffers from the fact that no long-range order exists and, in consequence, a statistical approach is more adequate. In a treatment of $E_2PI_{1\cdot6}$ Endres (1980) and Endres, Pouget & Comès (1982) (EPC hereafter) also report superorder phenomena in both substructures. As well as the Bragg peaks and the characteristic main diffuse layer line system of the iodine chains there are sharp satellite reflections $\pm 0{\cdot}27\, c_o^*$ around the Bragg layers and satellites with wavevectors $\mathbf{q} = (\pm\frac{1}{4}, \mp\frac{1}{4}, 0)$ in the first Bragg sheet indicating a modulation of the organic matrix. At low temperatures also diffuse sheets appear midway between the diffuse layer lines, which were scarcely detectable at room temperature. From intensity modulations within the diffuse layers EPC conclude that the average iodine positions are correlated at room temperature (RT) while lateral correlations between $I_3$ groups occur at low temperatures, too. Very weak diffuse lines were assigned to a second type of iodine chains with a period $c_1 \simeq 10{\cdot}4$ Å.

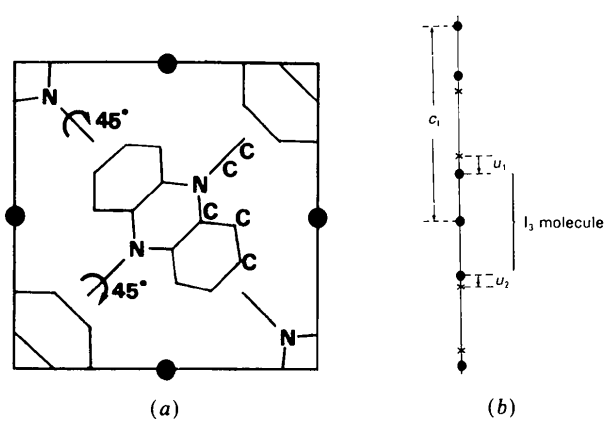


(*a*) (*b*)

Fig. 1. Schematic picture of the structure. (*a*) Projection on to the *ab* plane (after Endres, 1980). (*b*) Iodine chain: crosses indicate equidistant positions; $u_1$ and $u_2$ are shifts of the marginal atoms in one $I_3$ unit from these positions (see text).

Working on the same problem at the same time we made, surprisingly, some deviating observations, which we report here and compare with the results of EPC. For a quantitative analysis of the diffuse layer line system the intensity distributions at four different temperatures were also recorded very carefully. Diffuse X-ray scattering by iodine chains in various compounds has been analysed by several authors (Endres, Keller, Mégnamisi-Bélombé, Moroni, Pritzkow, Weiss & Comès, 1976; Scaringe & Ibers, 1979; Schramm, Scaringe, Stojakovic, Hoffmann, Ibers & Marks, 1980; Scaringe, Pace & Ibers, 1982; Filhol, Rovira, Hauw, Gaultier, Chasseau & Dupuis, 1979). An analysis of $E_2PI_{1\cdot6}$ in the frame of a Gaussian model was carried out by EPC. Comparably with their treatment we also describe the diffuse system in terms of 1D liquid, present two further models and compare all three at four different temperatures.

## 2. Experimental

The crystals used were synthesized by Dietz, University of Heidelberg. Because most of them were heavily twinned 'good' single crystals had to be selected in a tedious way. Dimensions of the 'best' needle-like crystals were $0{\cdot}2 \times 1$ mm in diameter and length,

respectively. It should be mentioned that our samples were deuterated (with a view to neutron experiments) which may be responsible for puzzling results (see § 3). In order to avoid a contamination of the diffuse background by Bragg-like phenomena as far as possible X-ray patterns were taken mostly by the Noromosic technique (non-rotating single crystal, monochromatic radiation). A cylindrically bent quartz monochromator crystal was used and the focal line was perpendicular to the camera axis parallel to which the long ($c$) axis of the crystal was chosen. By this, focusing on the film across the diffuse layer lines was achieved. With a short wavelength (Mo $K\alpha$) and an equi-inclination technique diffuse layer lines up to the 10th order are observable. This equi-inclination technique was also favourable with respect to a weak and smooth variation of the resolution volume, because the X-ray beam can be focused simultaneously on the 0th and the 10th diffuse layer. A schematic drawing of the scattering geometry with the symbols used is shown in Fig. 2.

The temperature of the sample was varied from 123 to 333 K in steps of 30 K by cooling or heating the specimen in a stream of nitrogen (cooling/heating stage Enraf-Nonius). The temperature of the sample during an exposure was stable within ±1 K; the accuracy on an absolute scale was better than ±2 K. Because of the hygroscopic character of the sample crystals and the temperature variation, the crystals were embedded in a drop of glue.

Before and after a cooling or heating treatment the quality of the sample crystal was checked by X-ray photographs taken at room temperature. All patterns were taken with the same setting of the crystal, the same exposure times (typically 12 h) and with the same operating conditions of a fine-focus X-ray tube (50 kV, 20 mA). The X-ray films were enveloped in Al foil to reduce the background due to fluorescence and air scattering as far as possible. During the developing process one side of the film emulsion was removed thus avoiding an artificial broadening of the measured profiles caused by the inclined incidence of the beam. Digital intensity data were then recorded by means of a 'flying-eye' microdensitometer in the usual way.

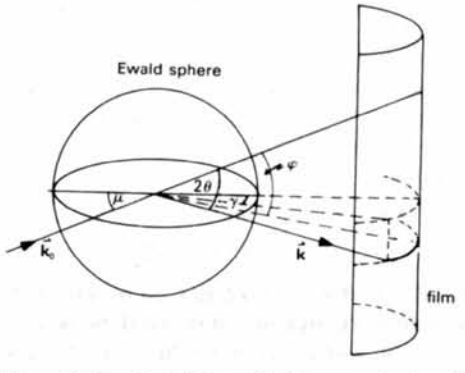


Fig. 2. Schematic drawing of the scattering geometry (equi-inclination angle $\mu$).

## 3. Scattering phenomena

### (*a*) *Observations at room temperature*

Fig. 3 shows a Noromosic photograph taken at 273 K. The scattering phenomena are separated into two parts corresponding to the two sublattices. On the left-hand side Bragg-like phenomena due to scattering of the organic part of the compound are indicated. The index $l$ is given here in units of $c_o^*$. The main Bragg reflections in sheets with $l$ = integer were used by Endres *et al.* (1979) for the determination of the averaged structure. A second set of sheets $\pm 0{\cdot}27\ c_o^*$ away from the Bragg-layers - also found by Endres *et al.* (1979) - is indicated by $l \pm 1$. These satellites are strong even around the 0th layer. On a Weissenberg photograph of this layer (0, +1) we found a quartet of satellites with vectors: $\mathbf{q}_{1/2} = (\pm 0{\cdot}5, 0, 0{\cdot}27)$ and $\mathbf{q}_{3/4} = (0, \pm 0{\cdot}5, 0{\cdot}27)$ (in units of $a^*$ and $c_o^*$, respectively). Fig. 3 further reveals the existence of second-order satellites at distances $\pm 0{\cdot}54 c_o^*$ not reported so far. One of these sheets (1, −2) is indicated.

On the right-hand side of the same figure all diffuse layers are marked by arrows; values of the index $l$ are now given in units of $c_I^*$ ($= 1/c_I$). The main system with integer $l$ values corresponds to the mean distance between the $I_3$ units and is incommensurate with the period of the organic sublattices. It was analysed by EPC quantitatively and is the topic of § 4. Without a detailed analysis it can be seen that a well ordered structure projected onto the *ab* plane exists (no diffuse sheet at $l = 0$). From the structural work we know that this projection forms a centred quadratic

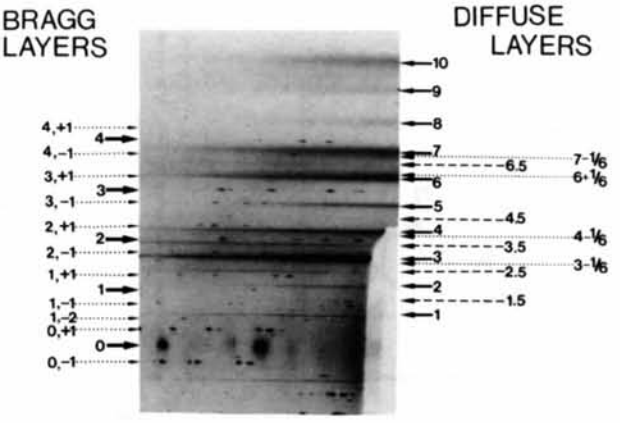


Fig. 3. X-ray photograph taken at 273 K; crystal orientation parallel to the $c$ axis; Mo $K\alpha$ radiation. Numbers represent $l$ indices given in units of $c_o^*$ (left-hand side) and $c_I^*$ (right-hand side).

net. Furthermore, no $00l$ reflections superimposed on the diffuse layers can be detected. Owing to the equi-inclination technique $00l$ reflections, if any, should be observed on the meridian of the photograph at least within the 8th to 10th layers. In the normal-beam technique $00l$ reflections remain unobservable.

The intensity distribution within the diffuse layers (main system) is not homogeneous. This is quite obvious from layer 3, but, in contrast to the communication of EPC, also from layers 1 and 2 (Fig. 3).

A Weissenberg photograph of the diffuse sheet at $l=3$ reveals the intensity distribution in more detail (Fig. 4): diffuse rods (or bands) run along $\langle\xi\xi\,0\rangle$ directions crossing one another at points $(hk3)$ with $h+k=2n$. The rod-like character was proved by densitometer scans (not shown here). In addition, weak, more or less diffuse, satellite reflections surround the midpoints of the intersections of the diffuse rods. With a view to a quantitative analysis of the diffuse distribution these short-range-order effects cannot be neglected.

A relatively strong second set of diffuse layer lines is located at positions $\pm c_1^*/2$ around the main layers. These layer lines were 'hardly detectable' at room temperature by EPC. Within these layers intensity concentrations occur also. They are definitely not due to a $\lambda/2$ contamination of the beam. We observe a remarkable extinction by inspection of the layer $l=6{\cdot}5$, where a 'hole' around the meridian $(00\zeta)$ is clearly visible.

These observations at RT are not in agreement with those of EPC who found in the sheet $l=3$ (and only there) 'broad maxima consisting of a diffuse maximum at integral values of $h$, surrounded by broad peaks centred at about $\eta=0{\cdot}22$ along the $\langle\eta\eta0\rangle$ reciprocal directions'. We observe the modulation also in other layers and identify the diffuse maxima with the intersection of diffuse rods; the satellites (*cf.* Fig. 4) are relatively sharp as compared with this diffuse maximum, and, finally, the satellite vectors are found to be $\mathbf{q}_{1/2}=(\pm1/3, 0, 0)$ and $\mathbf{q}_{3/4}=(0, \pm1/3, 0)$, respectively. It should be pointed out that $0{\cdot}22\times\sqrt{2}\times a^*\approx1/3\times a^*$. In our photographs the intensity distribution along $\langle\xi00\rangle$ is therefore characterized by a broad maximum, relatively sharp side peaks and a low background, whereas along $\langle\eta\eta0\rangle$ - running along a rod - we have a broad maximum and a high background. These distributions are not consistent with those communicated by EPC (see Fig. 14 therein). This discrepancy, however, cannot be solved by a simple 45° rotation of reciprocal axes.

A third system of diffuse layer lines is satellite sheets separated $\pm1/6c_1^*$ from the main diffuse layers. These satellite sheets obviously correspond to the 'very faint additional diffuse lines' reported by EPC to exist in front of the 3rd and the 4th diffuse layer at RT. We found these layers around the 3rd, 4th, 6th and 7th layers (*cf.* Fig. 3). An extinction as mentioned above does not hold in the case of the '$\frac{1}{6}$ system'.

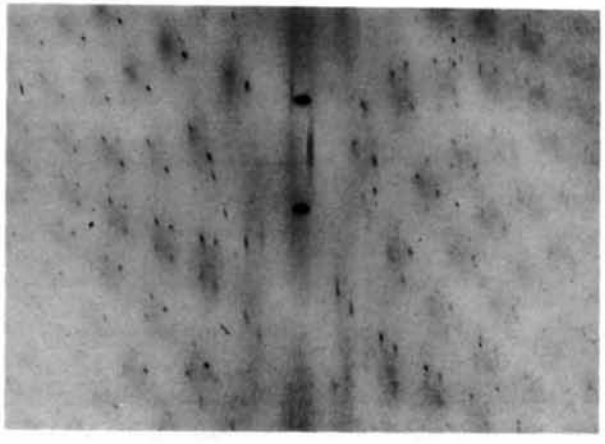

Fig. 4. Weissenberg photograph of the third diffuse layer (300 K).

### (*b*) *Temperature dependence*

Noromosic photographs at high and low temperatures (Fig. 5) reflect mostly a gradual change in the phenomena observed at RT. Restricting the discussion to the diffuse layers we found a sharpening of the layers parallel to $c_1^*$ and a considerable reduction of the diffuse background with decreasing temperature. The intensities of the sheets at $\pm c_1^*/2$ and $\pm c_1^*/6$ become more pronounced and are easily separated from the diffuse background as well as from the main system at temperatures below 150 K (*cf.* Fig. 6). The extinction concerning the layer lines of type $c_1^*/2$ is valid also at low temperatures as can be seen on Fig. 5(*b*). In particular, on the photograph taken at 123 K - a selected area of which is shown in Fig. 7 - we observe new diffuse lines at all positions $\pm\frac{1}{6}$, $\pm\frac{2}{6}$, ... or, in other words, satellite sheets of higher order. On the same figure the enhanced intensity modulation within all diffuse layers is obvious. A detailed study of the intensity concentrations within the different diffuse layers was not performed. From a brief inspection of Fig. 7 a new kind of scattering could be suspected, namely rods across the layer lines; these, however, might be simulated by a series of narrowly spaced Bragg spots.

### (*c*) *Discussion*

Longitudinal ordering (*i.e.* parallel to **c**) of the chains is mainly of short-range type (see § 4). Two superperiods along the chain direction are superimposed: one has a doubled, the other a sixfold period (in units of $c_1$). Both are of different origin because a characteristic extinction could only be observed in the first case. Vanishing intensity around the meridian $(00\zeta)$, in particular at sheets with higher $l$ indices, indicates shifts perpendicular to the modulation

wavevector. One simple explanation would be a tilt of the linear $I_3$ molecules with respect to the chain direction in a zigzag-like arrangement. On the other hand, a superperiod of $2c_1 = 19{\cdot}40$ Å is very close to $c_o/0{\cdot}27 = 19{\cdot}74$ Å which corresponds to the $c$ component of the satellite sheets around the Bragg layers. As discussed by Endres (1980) superstructure phenomena within the organic part could be due to different tilt angles in neighbouring stacks of the planar $E_2P$ cations or to shifts of these molecules within one stack parallel or transverse to the stacking (=**c**) direction. Although for a quantitative explanation more experimental information is needed, the relatively strong satellites around $l = 0$ indicate that the modulation of the stacking has no pure displacive character. Nevertheless, a coupling of the sublattices would provide a common modulation along **c**. Because the intensity of the diffuse layers in question and of the satellite sheets becomes more intense and, additionally, satellite layers of higher order occur at lower temperatures (*cf.* Fig. 7), the modulation becomes more pronounced, presumably due to stronger correlations between the iodine chains and the organic stacks.

The second modulation wave with a wavelength six times the chain period is observable also at room temperature and becomes obviously stronger at lower temperatures (*cf.* Fig. 6). Simultaneously diffuse sheets of higher order corresponding to this superstructure phenomenon were found (*cf.* Fig. 7). From our observations there is no reason to assign these extra lines to a second family of iodine chains with a different period of 10·4 Å (*cf.* also Fig. 5) as was done by EPC. As mentioned a comparison of the

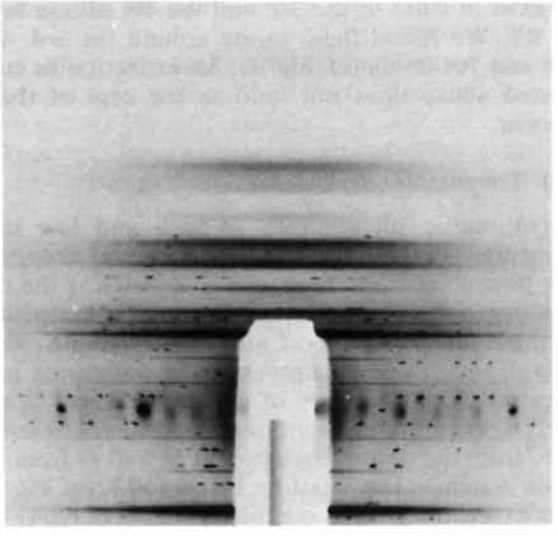

(*a*)

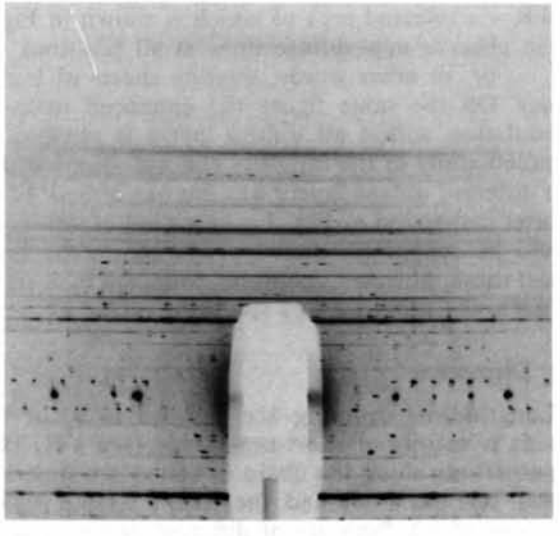

(*b*)

Fig. 5. X-ray photographs (Noromosic technique) taken at (*a*) 333 K and (*b*) 123 K; Mo $K\alpha$ radiation; focusing on the 0th and the 10th diffuse layer simultaneously.

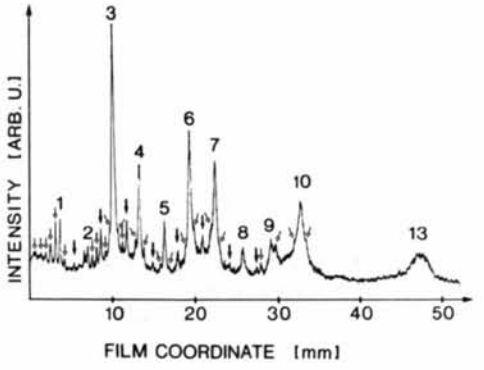


Fig. 6. Microdensitometer scan of Fig. 5(*b*); scan direction perpendicular to the layers. Numbers indicate the $l$ indices of the main diffuse layer lines. Full arrows point at layer lines with $l \pm \frac{1}{2}$, open arrows show positions $\pm\frac{1}{6}n$ around the main layer-line system.

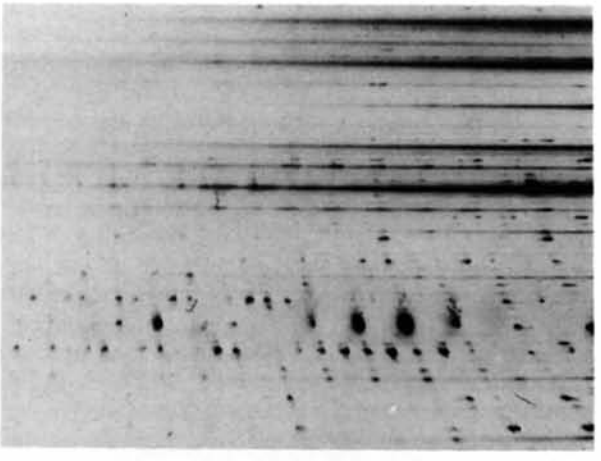

Fig. 7. Magnified selected area of a Noromosic photograph taken at 123 K.

intensities around the meridian shows that this type is different from that discussed before. Purely formally one can derive a common $c$ period of $11c_o \approx 6c_I \approx 58$ Å for both sublattices at least at low temperatures and interpret this as a kind of commensuration or resonance between the sublattices. It might also be simulated by an accidental superposition of Bragg spots and a diffuse layer within the limit of the instrumental resolution.

Concerning the lateral behaviour, EPC derive an ordering between the *average* iodine positions at RT, while absent intensity modulations within the 6th diffuse layer were explained as being of short-range type. In their picture a radial projection of the iodine strings onto the $c$ axis would lead to an averaged (projected) structure and, in consequence, to *sharp* $00l$ reflections (in units of $c_I^*$) superimposed on the diffuse sheets. By our scattering technique we should observe at least one or two of them, but could not detect any. Instead from our findings we deduce lateral correlations between the *actual* positions of $I_3$ groups similar to that of $B_2PI_{1\cdot6}$ as reported by EPC.

Corresponding to the diffuse rods within the layers these correlations are due to short-range interactions between the chains within (110) planes, *i.e.* perpendicular to the N–N directions of the $E_2P$ molecules. The extinction rule for the diffuse rods reflects, of course, the lateral arrangement of the iodine chains within these planes $\frac{1}{2}|\mathbf{a}+\mathbf{b}|$ apart. From the width of the rods a correlation length of $(3/\sqrt{2})\ a \approx 26$ Å can be estimated. The origin of the subsidiary, relatively sharp peaks along $(\xi 00)$ directions at $\xi = \frac{1}{3}$ has not been investigated so far. However, we cannot confirm the conclusions of EPC, who discuss a local order along [110] (in direct space) with a periodicity of roughly four interchain distances. They suppose 'a local phase shift in chain directions of chains, possibly brought about by repulsive Coulomb interactions between them'. This mechanism was discussed in the case of $Hg_{3-\delta}AsF_6$ at low temperatures (Pouget, Shirane, Hastings, Heeger, Miro & MacDiarmid, 1978). Because we observe the modulation along **a** (or **b**), correlations between iodine chains can exist only *via* interactions of iodine chains and $E_2P$ stacks indicating a stronger coupling between the organic part and the iodine strings.

Lateral interactions become stronger at low temperatures and, in consequence, correlations extend over greater distances. A real phase transition of any kind was not observed within the range of our temperature variation down to 123 K (in agreement with EPC). We have discussed the phenomena qualitatively only, because the experimental data at hand do not allow a quantitative model description. In this respect we would need more information, in particular about the precise intensity distributions within the diffuse satellite sheets which are very weak. This work is currently in progress.

## 4. Quantitative analysis of the main diffuse system

### (*a*) *One-dimensional liquid models*

The interpretation in terms of 1D liquids is strongly suggested by the characteristic damping of the intensity and the increase of the line widths with higher scattering angles. Another approach would be a dynamical model in terms of 1D longitudinal modes, discussed *e.g.* by Emery & Axe (1978) for Hg chains in $Hg_{3-\delta}AsF_6$. Since, however, at present we have no information as to whether the scattering is elastic or inelastic (neutron scattering experiments are planned to clarify this point), the quantitative evaluation will here be carried out for simple 1D liquid models only, since similar interference functions are expected for both approaches [*cf.* Emery & Axe (1978) and EPC].

Some preliminary remarks should clarify the term 'one-dimensional' crystal or liquid, since it is used in different ways in the literature. In a strict sense a 1D crystal is defined as having translational symmetry in only one direction. The corresponding reciprocal lattice consists of a set of parallel equally spaced and equally sharp planes perpendicular to the direction of repetition, the intensity variation in this direction being given by the structure factor of a basic chain unit. If the centres of these units are additionally located on parallel equidistant *ab* planes, the projected structure onto a line parallel to the unique **c** direction is well ordered, leading to sharp $00l$ reflections superimposed on the planes. On the other hand, the chains themselves may form a well ordered 2D lattice, such that the projection on the *ab* plane shows only sharp $hk0$ reflections (*i.e.* there is no sheet for $l = 0$). In any case, as long as a mean repeat distance does exist, any random disorder in the **c** direction does not affect the overall diffraction pattern apart from a (static) Debye–Waller factor, *i.e.* the planes remain sharp. In our case, however, the fact that the widths of the planes increase more strongly than linearly with $l$ (approximately $\Delta l \sim l^2$; see Fig. 8 of EPC) rules out the possibility of a crystalline behaviour including particle-size ($\Delta l =$ constant) or strain ($\Delta l \sim l$) effects. Thus the long-range order within the chains is lost, leading to a liquid- or amorphous-like arrangement. As there are no sharp $00l$ reflections and no diffuse sheet for $l = 0$, the liquid character is clearly in the direction of the chains, which are well ordered in the *ab* plane.

The electron distribution along **c** can be written as the convolution $\rho(z) = \rho_m(z) * S(z)$, where $\rho_m(z)$ is the distribution within the molecule and $S(z)$ the distribution of the molecules along the chain direction. Neglecting the effect of the form factor and the temperature factor in the $a^*b^*$ plane (components $\xi, \eta$), as well as any lateral ordering between the chains, the scattered intensity has only $\zeta$ dependence, $\zeta$ being the component of the scattering vector in the

direction of $\mathbf{c}^*$:

$$I(\zeta) = \mathscr{F}\{\rho(z) * \rho(-z)\}$$
$$= |\mathscr{F}\{\rho(z)\}|^2 = |\mathscr{F}\{\rho_m(z)\}|^2 \,.\, |\mathscr{F}\{S(z)\}|^2$$
$$= |F(\zeta)|^2 \,.\, G(\zeta). \qquad (1)$$

$F(\zeta)$ is the 1D structure factor of the $I_3^-$ unit and $G(\zeta)$ the 1D intermolecular interference function of the chains. In the scattering geometry we used $\zeta = (2/\lambda)\sin(\varphi/2)\,.\cos[(\varphi/2)-\mu]$ (see Fig. 2).

There are several possibilities for deriving an analytic expression for $S(z)$ or $G(\zeta)$. Probably the best known result is that of Zernike & Prins (1927) (ZP) for 1D liquids, who consider a random distribution of $N$ small rods of length $a_o$ along a line of length $L(\to\infty)$ with a mean distance between the ends of neighbouring rods $\sigma_o = (L - Na_o)/N$. Their result is:

$$G(\zeta) = \{2\pi^2\delta_o^2\zeta^2\}/\{1+2\pi^2\delta_o^2\zeta^2 - [\cos(2\pi a_o\zeta) - 2\pi\delta_o\zeta\sin(2\pi a_o\zeta)]\}. \qquad (2)$$

The mean distance between the centres of the rods is given by $\bar{d} = a_o + \delta_o$.

Here we adopt the more general paracrystal method [Hosemann (1950); see also Vainshtein (1966) and references therein]. This method starts with the distribution function $h_1(z)$ of the first neighbours of an arbitrary reference unit. Assuming centrosymmetry $h_1(z) = h_{-1}(-z)$ and regarding a normalized function $\int_{-\infty}^{+\infty} h_1(z)\,dz = 1$, the mean distance between two neighbouring units is $\bar{d} = \int_{-\infty}^{+\infty} z h_1(z)\,dz$. Then the function describing the distribution of the $m$th neighbour with respect to the reference one is given by an $m$-fold convolution

$$h_m(z) = h_1(z) * h_1(z) * \ldots * h_1(z) = \int_{-\infty}^{+\infty} h_1(z') \,.\, h_{m-1}(z-z')\,dz'.$$

Hence the total distribution function is

$$S(z) = \delta(z) + \sum_{m=1}^{\infty} [h_m(z) + h_{-m}(z)]$$

and by Fourier transformation we obtain

$$G(\zeta) = \mathscr{F}\{\delta(z)\} + \mathscr{F}\left\{\sum_{m=1}^{\infty}[h_m(z)+h_{-m}(z)]\right\}$$
$$= 1 + \sum_{m=1}^{\infty}[H^m(\zeta) + H^{*m}(\zeta)]$$
$$= 1 + 2\,\mathscr{R}e\,\{H(\zeta)/[1-H(\zeta)]\}, \qquad (3)$$

where we have defined $H(\zeta) = \mathscr{F}\{h_1(z)\}$ and $\mathscr{R}e$ is the real part of the expression.

A physical model can now be introduced by specifying $h_1(z)$. In principle this has to be found from the interaction forces between next neighbours. A reasonable potential should include a 'rigid-body' repulsive part and a 'van der Waals' attractive part. For a quantitative comparison with the measured diffuse intensity variation we examined three different models.

(1) $M1$:

$$h_1'(z) = \begin{cases} \dfrac{1}{\sigma_1} e^{-(z-c_o)/\sigma_1} & \text{for } z \geq c_o \\ 0 & z < c_o. \end{cases} \qquad (4a)$$

This strongly asymmetric function describes a kind of 'hard-sphere' model with a shortest distance $c_o$ and a characteristic width $\sigma_1$ {equal to the r.m.s. deviation $\Delta d = [\overline{(z-\bar{d})^2}]^{1/2}$}.

$$H'(\zeta) = \frac{1}{1-2\pi i\zeta\sigma_1} e^{+2\pi i c_o\zeta} \qquad (4b)$$

$$G'(\zeta) = \{2\pi^2\zeta^2\sigma_1^2\}/\{1+2\pi^2\zeta^2\sigma_1^2 - [\cos(2\pi c_o\zeta) - 2\pi\zeta\sigma_1\sin(2\pi c_o\zeta)]\}. \qquad (4c)$$

Identifying $c_o$ with $a_o$ and $\sigma_1$ with $\delta_o$ we immediately see that this result reproduces the ZP model [equation (3)] which is of course a consequence of the identical physical models. Again the mean distance $\bar{d} = c_o + \sigma_1$.

(2) On the other hand, we may start with a mean distance $\bar{d} = c_o$ and a totally symmetric Gaussian distribution of width $\sigma_2 (= \Delta d)$ around it:

$M2$:

$$h_1''(z) = \left(\sqrt{\frac{2}{\pi}}\right)\left(\frac{1}{\sigma_2}\right) e^{-(z-c_o)^2/2\sigma_2^2} \qquad (5a)$$

$$H''(\zeta) = e^{-2\pi^2\sigma_2^2\zeta^2}\, e^{2\pi i c_o\zeta} \qquad (5b)$$

$$G''(\zeta) = \frac{1 - e^{-4\pi^2\sigma_2^2\zeta^2}}{1 - 2\,e^{-2\pi^2\sigma_2^2\zeta^2}\cos 2\pi c_o\zeta + e^{-4\pi^2\sigma_2^2\zeta^2}}. \qquad (5c)$$

This function has been used by EPC in their interpretation of the diffuse layer system.

(3) A 'weak' hard-sphere model would involve a mean shortest distance $c_o$ and take into account some flexibility of the $I_3$ molecule. Such a slightly asymmetric distribution can be obtained by a convolution of $h_1'$ with a Gaussian:

$M3$:

$$h_1'''(z) = \left(\sqrt{\frac{2}{\pi}}\right) \times \left(\frac{1}{\sigma_1\sigma_2}\right) \int_{c_o}^{\infty} e^{-(z'-z)^2/2\sigma_2^2}\, e^{-(z'-c_o)/\sigma_1}\,dz' \qquad (6a)$$

$$H'''(\zeta) = \frac{1}{1-2\pi i\sigma_1\zeta} e^{-2\pi^2\sigma_2^2\zeta^2}\, e^{2\pi i c_o\zeta} \qquad (6b)$$

$$G'''(\zeta) = \{1 + 4\pi^2\sigma_1^2\zeta^2 - e^{-4\pi^2\sigma_2^2\zeta^2}\}/$$
$$\{1 + 4\pi^2\sigma_1^2\zeta^2 - 2\,e^{-2\pi^2\sigma_2^2\zeta^2}$$
$$\times[\cos 2\pi c_o\zeta - 2\pi\sigma_1\zeta \sin 2\pi c_o\zeta] + e^{-4\pi^2\sigma_2^2\zeta^2}\}. \quad (6c)$$

Here the sharp cut-off at $z = c_o$ in $M1$ is avoided by a distribution of the shortest distances $c_o$ with width $\sigma_2$, while, as before, the asymmetry is governed by $\sigma_1$. The mean distance is $\bar{d} = c_o + \sigma_1$ and the r.m.s. deviation $\Delta d = \sqrt{\sigma_1^2 + \sigma_2^2}$. The three different distribution functions are compared in Fig. 8 (for our results at RT).

### (*b*) *Data reduction*

In order to compare the results for $G(\zeta)$ with the measured intensity variation some corrections have to be made. First, the diffuse layers show some modulations due to moderate lateral short-range-order effects, which become more pronounced at low temperatures. However, because the integrated scattered intensity of a given assembly of atoms remains unchanged during ordering processes these modulations can be averaged out. The whole 2D data set corresponding to one Noromosic photograph was therefore divided into strips perpendicular to **c***. Each of these 1D data sets parallel to the layer lines was then smoothed by cubic spline functions. Of course there remains an overall decrease due to a form and temperature factor. An example is shown in Fig. 9. The extent of smoothing is governed by a weighting factor, which was defined (at each temperature) from a section along the third diffuse layer line and then held fixed for the whole data array. The intensity distribution parallel to **c*** was then extracted by an appropriate section across the smoothed profiles. Regions where Bragg and satellite reflections contaminate the profiles were omitted (missing points in Fig. 11).

For each temperature these intensity distributions were compared with the calculated intensities $y$(calc) for the three different models by using a least-squares fitting procedure. $y$(calc) is given by equations (4*c*), (5*c*), (6*c*) corrected by a polarization factor $P$ and an absorption factor $A$, and convoluted with the resolution function R of the instrument:

$$y(\text{calc}) = |F_1|^2 G(\zeta) PA * R.$$

The structure factor $F_1$ is (*cf.* Fig. 1*b*)

$$F_1(\zeta) = f_j(\zeta) \sum_{j=1}^{3} \exp\left\{-B_j\left(\frac{\sin\theta}{\lambda}\right)\right\} \times \cos[2\pi(\zeta/\bar{d})(\tfrac{1}{3} - u_j)];$$
$$u_3 = \tfrac{1}{3}; \qquad B_1 = B_2.$$

The $\zeta$ dependence of $f_j$ was approximated by the usual series expansion in exponentials (*cf. International Tables for X-ray Crystallography*, 1962). We also tried the acentric case $u_1 \neq u_2$, but did not find any significant improvement of the fit, *i.e.* the $I_3$ molecule is really symmetric.

The relatively high mean linear absorption coefficient of the compound $\mu_A = 31{\cdot}5\ \text{cm}^{-1}$ (evaluated from data given in *International Tables*, 1962) demands a correction too. However, no simple correction factor exists for the scattering geometry used. A general method of Wünsch & Prewitt (1965) was used. Rather lengthy expressions can be derived and will be discussed elsewhere [Rosshirt (1982, and to be published)]. The correction factors were tabulated as a function of the angles $\varphi$ and $\gamma$ and used pointwise.

The convolution with the normalized resolution function $R(\xi - \xi', \eta - \eta', \zeta - \zeta')$ deserves special attention. Since R is integrated by the diffuse sheets in $\xi, \eta$ directions, we have only to consider the $\zeta$ dependence. For a discussion of the relation between R and the usual Lorentz factor see Boysen & Adlhart (1983). R may, *e.g.*, be deduced from the Bragg reflec-

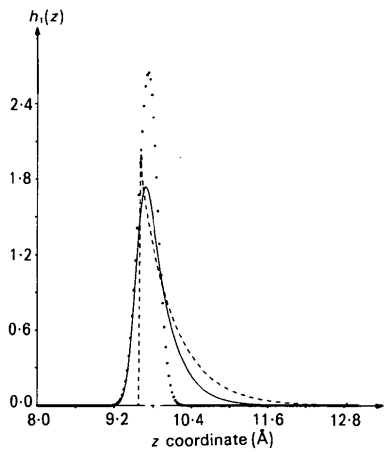


Fig. 8. Normalized distribution functions $h_1(z)$ for all three models discussed in the text. $M1$: - - - $M2$: ■■■■ $M3$: ——.

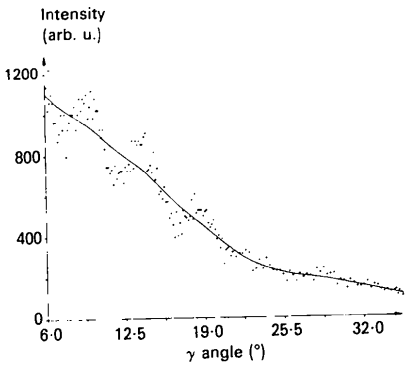


Fig. 9. Intensity distribution within the third diffuse layer showing an overall decrease and, in addition, short-range-order peaks. The solid line results from a procedure averaging out this lateral short-range-order effect (see text). For an explanation of angle $\gamma$ see Fig. 2.

tions as they are $\delta$ functions and thus a direct measure of R. As can be seen from the photographs (Fig. 5), to a first approximation the $\zeta$ dependence is independent of $\xi$ and $\eta$. We therefore analysed a total of 115 Bragg reflections; all reveal a marked asymmetry. Several functions have been tried to fit the Bragg profiles; the best results were obtained for asymmetric Gaussians

$$R(\zeta-\zeta') = \exp\{-4\ln 2(\zeta-\zeta')^2/\beta^2\} \times[1-P(\zeta-\zeta')^2\,\mathrm{sign}\,(\zeta-\zeta')],$$

where $\beta$ governs the width and $P$ the degree of asymmetry. While $P$ was found to be constant over the whole pattern, $\beta$ depends on $\varphi$ and could be fitted to a polynomial of second degree in tg $\varphi/2$, which is also valid for other scattering geometries.

A serious problem is the background separation. It can be estimated from $\zeta$ points where $F_I = 0$. In between these points the background may be found by linear interpolation. However $F_I$ itself is a function of the fitted parameters. Hence, these particular points have to be redetermined after each cycle and, in consequence, the background re-evaluated. The second point concerns the zero line $\zeta = 0$, which cannot be taken directly from the film. This is due to the inclination technique and to the fact that the Bragg reflections on the 0th layer line are heavily overexposed and therefore very broad. This was accounted for by introducing a fit parameter $\zeta_o$. One further parameter $\mu_o$ relies on the uncertainty of the equi-inclination angle $\mu \approx 21{\cdot}7°$.

### (c) *Results*

$M1$ and $M2$ are special cases of $M3$ with $\sigma_2 = 0$ and $\sigma_1 = 0$, respectively, as can be seen by comparing (4*c*) and (5*c*) with (6*c*). Thus there is a total of nine or eight parameters, respectively, which have to be refined during the fit: the distribution parameters $c_o$, $\sigma_1$ and $\sigma_2$, the structural parameters $u_1$, $B_3$ and $B_1$ and the parameters $\zeta_o$, $\mu_o$ and $c$ (scaling factor).

At all temperatures the profile $R_p$ factors are clearly the lowest for $M3$ (*cf.* Table 1). Moreover, the significance levels (Hamilton, 1965) in favour of $M3$ are >99·5%. The final values of all essential parameters for $M3$ are given in Table 2. The corresponding temperature dependence of the distribution function $h_1'''(z)$ is plotted in Fig. 10 and the observed and calculated intensities are compared in Fig. 11. The structural parameter $u_1$ is independent of temperature within the e.s.d.'s, and, moreover, independent of the model. This, of course, reflects the fact that the structure factor is not much influenced by the chosen statistic function. The thermal parameters $B_3$ and $B_1 = B_2$ differ markedly from one another, indicating larger vibrational amplitudes of the marginal atoms. There is an expected overall decrease with decreasing temperature with the exception of the fit at the lowest temperature of 183 K. This is connected with the invalidity of the model at low temperatures and will be discussed below. The same general behaviour was found for $M1$ and $M2$, where, however, the absolute values are higher for $M2$ ($B_3 \approx 3{\cdot}4 \rightarrow 2{\cdot}5$ Å$^2$, $B_1 \approx 4{\cdot}4 \rightarrow 3{\cdot}3$ Å$^2$) but unrealistically low for $M1$ ($B_3 \approx 0{\cdot}3 \rightarrow 0{\cdot}0$ Å$^2$, $B_1 \approx 1{\cdot}1 \rightarrow 0{\cdot}3$ Å$^2$). The difference $B_1 - B_3 \approx 0{\cdot}7 - 0{\cdot}9$ Å$^2$ is approximately constant in each case, *i.e.* it seems to reflect the real difference between the amplitudes of the central and the marginal atoms, while the different absolute values of $M1$ and $M2$ simply account for the different statistics of the whole molecule.

In contrast, the variation of the mean distance $\bar{d}$ with temperature (Fig. 12*a*) favours $M1$ or $M3$. Both show the normal expected behaviour of an expanding lattice, while there is an unrealistic decrease for $M2$. Taking together the behaviour of $B$ and $\bar{d}$, we thus have another strong hint in favour of $M3$. The r.m.s. deviation $\Delta d$ decreases with decreasing temperature in all three models as shown in Fig. 12(*b*). The slope in $M2$ is remarkably smaller than in $M1$ or $M3$, while the absolute value is again intermediate for $M3$. Although it is difficult to favour one of them on plausible physical grounds, one can suspect that the different values of $M1$ and $M2$ are corrected partly by the opposite behaviour of the $B$ parameters.

Some remarks should be made concerning the results of EPC in comparison to ours on the identical $M2$. Although there is a gross agreement for $c_o$ and $u_1$, there appears to be a discrepancy in the values of $\sigma_2$, which in our evaluation is lower by about a factor of two. This again might be due to their smaller value of $B$. In their calculations they obviously varied only $u_1$ and $\sigma_2$, keeping $c_o = 9{\cdot}70$ Å and $B = 2{\cdot}6$ Å$^2$ (only one for all atoms) fixed. EPC claim a linear dependence of $\sigma_2^2$ *versus* $T$ at high temperatures accounting for 1D dynamical fluctuations of longitudinal acoustic modes in the harmonic approximation. Our results, however, point more towards a linear dependence of $\Delta d$ on temperature (for all three models) between $T = 183$ and 293 K and only a slight decrease at the highest measured temperature, 333 K. It should be mentioned that the results of EPC equally well fit a linear $\sigma_2$ *vs* $T$ dependence as shown in Fig. 12(*b*) with a slope nearly identical to that of $M2$. Although a clear-cut distinction should not be made on the basis of only a few observations, the fact that the best distribution function shows a pronounced asymmetry suggests that the harmonic approximation is no longer sufficient.

Obviously the fits become worse at low temperatures as seen from Table 1 and Fig. 11 (no fits were tried for $T < 183$ K), indicating that the 1D liquid model becomes inadequate at low temperatures. The $B$ values at 183 K probably contain some of the deviations towards a more ordered model. The increasing long-range order (decreasing $\Delta d$ with

Table 1. *Final $R_p$ factors (%) for all models discussed in the text*

| $T$(K) | 333 | 303 | 243 | 183 |
|---|---|---|---|---|
| $M1$ | 7·7 | 8·2 | 10·5 | 13·9 |
| $M2$ | 7·6 | 7·9 | 9·6 | 11·3 |
| $M3$ | 6·8 | 7·6 | 8·8 | 11·1 |

Table 2. *Final parameters of model M3 at four temperatures*

| $T$(K) | 333 | 303 | 243 | 183 |
|---|---|---|---|---|
| $u_1$ | 0·029(3) | 0·029(3) | 0·032(2) | 0·028(3) |
| $B_3$(Å$^2$) | 1·27(13) | 1·09(12) | 1·01(20) | 2·11(27) |
| $B_1$(Å$^2$) | 2·19(12) | 1·79(11) | 1·69(14) | 2·72(22) |
| $c_o$(Å) | 9·539(7) | 9·547(6) | 9·609(5) | 9·655(9) |
| $\sigma_1$(Å) | 0·34(1) | 0·32(1) | 0·24(1) | 0·15(1) |
| $\sigma_2$(Å) | 0·128(3) | 0·114(3) | 0·099(2) | 0·079(2) |
| $\bar{d}$(Å) | 9·87(1) | 9·86(1) | 9·84(1) | 9·80(1) |
| $\Delta d$(Å) | 0·36(1) | 0·34(1) | 0·26(1) | 0·17(1) |

decreasing $T$) should not lead to a phase transition at $T>0$ K. However, with decreasing temperature lateral correlations between the chains as well as correlations with the organic host structure grow, *i.e.* a pure 1D model must fail at low temperatures.

## 5. Discussion

As to the discrepancies with EPC we have to suppose that our samples are in a different state of order concerning the superstructure phenomena although our crystals were synthesized in the same laboratory. One possible explanation could be a 'freezing' of $E_2PI_{1\cdot6}$ in different metastable (super)structural variants during the crystal-growth process. The only true difference to the best of our knowledge is the deuteration of the sample. This would indicate a remarkable influence of hydrogen bonding and therefore a considerable influence of the organic part of the structure on the ordering behaviour of the iodine chains. Beyond this we may conclude from our observations that the formal separation of the scattering phenomena into two parts is an oversimplification. Despite the incommensurability of both sublattices a mutual influence *via* common superperiods and, in consequence, mutual intensity contributions to the satellite scattering of either type cannot be ignored.

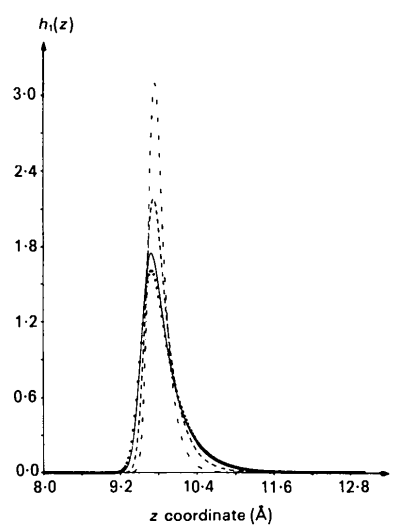


Fig. 10. Variation of $h_1(z)$ of $M3$ with temperature. 333 K: ■■■■, 303 K: ——, 243 K: - - - -, 183 K: - · - · - ·.

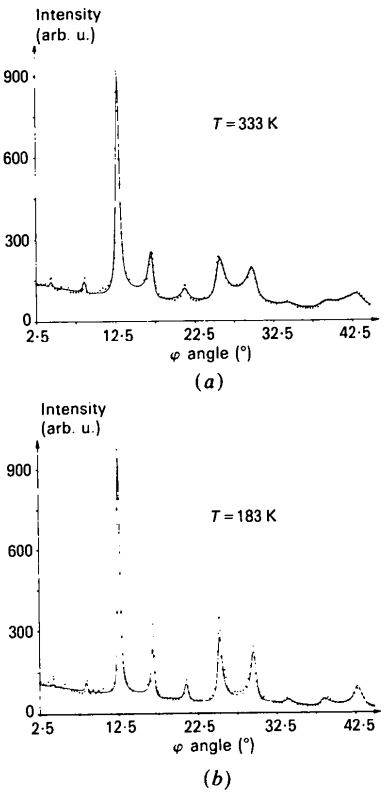


Fig. 11. Results of the fitting to model $M3$ described in the text [(*a*) 333 K and (*b*) 183 K]. Each third experimental point is plotted only. Angular intervals with omitted points belong to regions where the diffuse intensity would be contaminated by Bragg and satellite reflections from neighbouring layer lines.

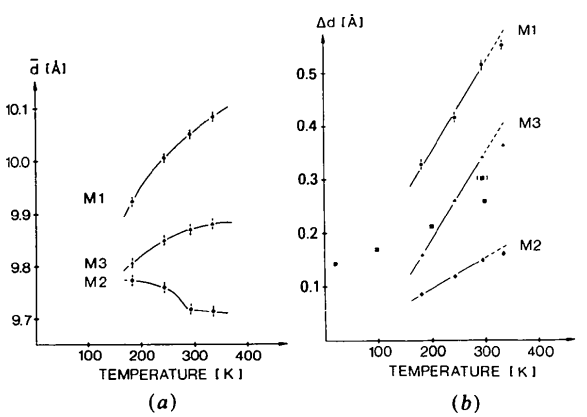


Fig. 12. Temperature dependence of (*a*) mean distance $\bar{d}$ and (*b*) r.m.s. deviation $\Delta d$, respectively, for all three models. In (*b*) results of EPC are included for comparison (■).

This has to be taken into account in a renewed precise structure refinement. In the quantitative analysis of the diffuse layers the main difference of our model $M3$ in comparison with the calculations of EPC (equivalent to our $M2$) is the asymmetry of the distribution function, which implies a shortest distance between the terminal atoms of adjacent molecules. This value is about 3·44 Å, which is considerably shorter than the van der Waals distance (4·2 Å) found in other I compounds (including those containing isolated $I_3^-$ molecules), with the exception of $N(CH_3)_4I_5$, where the shortest distance is 3·55 Å (Broekema, Havinga & Wiebenga, 1957). Moreover, there seems to exist a critical distance $D = 5{\cdot}80$ Å between the marginal atoms within one molecule, below which it is symmetric, whereas it is asymmetric ($u_1 \neq u_2$) for larger values (Mooney-Slater, 1959). Thus here one would expect an asymmetric molecule ($D = 5{\cdot}92$ Å) in contrast to the results. From all this we have to conclude that there are no 'isolated' $I_3^-$ molecules, *i.e.* there is chemical bonding between them beyond van der Waals forces. This can be explained by a partial delocalization of the electrons, thus accounting for the moderate metallic character of the compound in accordance with the findings of Endres (1980) that the electrical conductivity is due to the iodine chains, and not to the organic stacks. Therefore, the term 'liquid' should not be taken too literally, although the general behaviour is similar, since there are two stronger bonds alternating with one weaker bond being reflected by the 'smeared out' asymmetric distribution function. Correspondingly, in the dynamical approach one has to consider two different interaction forces between the atoms. A more sophisticated description should consequently also include anharmonic terms in the Debye-Waller factor. Furthermore, the formal separation between intra- and intermolecular interactions is an approximation only: any coordination statistics between $I_3^-$ units affects the internal structure of the $I_3^-$ molecule leading to a statistics of the structure factors too. Finally, we wish to mention that the whole discussion is based on purely static pictures. One cannot exclude, however, that (part of) the diffuse scattering is of inelastic origin. In this case dynamical processes have to be considered too.

The authors wish to express their gratitude to Dr Dietz (Univ. Heidelberg) for providing single crystals, and to Professor Huber, Dr Marquart (MPI Martinsried) and Dr Martin for experimental support. The work was supported by funds of the BMFT under 03-I02A04.

### References


BOYSEN, H. & ADLHART, W. (1983). *Z. Kristallogr.* **162**, 35-37.

BROEKEMA, J., HAVINGA, E. E. & WIEBENGA, E. H. (1957). *Acta Cryst.* **10**, 596.

EMERY, V. J. & AXE, J. D. (1978). *Phys. Rev. Lett.* **40**, 1507-1511.

ENDRES, H. (1980). Habilitation-Thesis, Univ. Heidelberg.

ENDRES, H., HARMS, R., KELLER, H. J., MORONI, W., NÖTHE, P., VARTANIAN, M. H. & SOOS, Z. G. (1979). *J. Phys. Chem. Solids*, **40**, 591-596.

ENDRES, H., KELLER, H. J., MÉGNAMISI-BÉLOMBÉ, M., MORONI, W., PRITZKOW, H., WEISS, J. & COMÈS, R. (1976). *Acta Cryst.* A**32**, 954-957.

ENDRES, H., POUGET, J. P. & COMÈS, R. (1982). *J. Phys. Chem. Solids*, **43**, 739-748.

FILHOL, A., ROVIRA, M., HAUW, C., GAULTIER, J., CHASSEAU, D. & DUPUIS, P. (1979). *Acta Cryst.* B**35**, 1652-1660.

HAMILTON, W. C. (1965). *Acta Cryst.* **18**, 502-510.

HOFFMANN, B. M., MARTINSEN, J., PACE, L. J. & IBERS, J. A. (1982). *Extended Linear Chain Compounds*, edited by J. S. MILLER. New York: Plenum.

HOSEMANN, R. (1950). *Z. Phys.* **128**, 1-35, 46-62, 465-492.

*International Tables for X-ray Crystallography* (1962). Vol. III. Birmingham: Kynoch Press.

MOONEY-SLATER, R. C. L. (1959). *Acta Cryst.* **12**, 187-196.

POUGET, J. P., SHIRANE, G., HASTINGS, J. M., HEEGER, A. J., MIRO, N. D. & MACDIARMID, A. G. (1978). *Phys. Rev. B*, **18**, 3645-3656.

ROSSHIRT, E. (1982). Diplomarbeit, Univ. München.

SCARINGE, R. P. & IBERS, J. A. (1979). *Acta Cryst.* A**35**, 803-810.

SCARINGE, R. P., PACE, L. J. & IBERS, J. A. (1982). *Acta Cryst.* A**38**, 608-611.

SCHRAMM, C. J., SCARINGE, R. P., STOJAKOVIC, D. R., HOFFMANN, B. M., IBERS, J. A. & MARKS, T. J. (1980). *J. Am. Chem. Soc.* **102**, 6702-6713.

VAINSHTEIN, B. K. (1966). *Diffraction of X-rays by Chain Molecules*. Amsterdam, London, New York: Elsevier.

WÜNSCH, B. J. & PREWITT, C. T. (1965). *Z. Kristallogr.* **122**, 24-59.

ZERNIKE, F. & PRINS, S. A. (1927). *Z. Phys.* **41**, 184-194.